2023

Comparison of Dynamics Stability Testing Techniques with Magnetic Suspension Wind Tunnel Capabilities

Otoniel A. Ramirez
NASA Langley Research Center

Mark Schoenenberger
NASA Langley Research Center

David E. Cox
NASA Langley Research Center

Colin P. Britcher
Old Dominion University

Original Publication Citation

Ramirez, O. A., Schoenenberger, M., Cox, D. E., & Britcher, C. P. (2023) *Comparison of dynamics stability testing techniques with magnetic suspension wind tunnel capabilities* [Paper presentation]. AIAA SciTech Forum, National Harbor, MD. https://doi.org/10.2514/6.2023-1817

AIAA SciTech Forum
23-27 January 2023, National Harbor, MD & Online
AIAA SCITECH 2023 Forum

10.2514/6.2023-1817

Comparison of Dynamic Stability Testing Techniques with Magnetic Suspension Wind Tunnel Capabilities

Otoniel Ramirez[1], Mark Schoenenberger[2], David E. Cox[3]
NASA Langley Research Center, Hampton, VA 23666

Colin P. Britcher[4]
Old Dominion University, Norfolk, VA 23529

Dynamic stability testing techniques currently utilized at NASA Langley Research Center (LaRC) are conducted in multiple facilities and consists of free flight, forced oscillation, and free-to-oscillate tests. The NASA/ODU Magnetic Suspension and Balance System (MSBS) has been recommissioned to explore its utility as an additional facility to expand the dynamic stability test capabilities currently available at NASA LaRC. Simulations were created to replicate each current test facility and method as closely as possible. Data collected from the simulated environments was corrupted with replicated noise sources of the different testing environments and then compared to real data collected during tests when such data was available. The corrupted data was then passed through data reduction and System Identification (SID) to estimate the accuracy of the results with the known aerodynamic model that was utilized within the simulation to generate the original data. Magnitudes of noise were varied utilizing Monte Carlo analysis to perform sensitivity analysis of each noise source on the extracted dynamic stability coefficients. Some preliminary results will be presented.

I. Nomenclature

A_{bb}	=	Accelerations in body-fixed axes
$\overline{B_{ll}}$	=	Magnetizing forces and gradients of the corresponding subscript
CG	=	Center of Gravity
CP	=	Center of Pressure
C_X	=	Aerodynamic force coefficient of the forces in the x-axis
C_Y	=	Aerodynamic force coefficient of the forces in the y-axis
C_Z	=	Aerodynamic force coefficient of the forces in the z-axis
C_l	=	Aerodynamic moment coefficient of the forces in the x-axis
C_m	=	Aerodynamic moment coefficient of the forces in the y-axis
C_n	=	Aerodynamic moment coefficient of the forces in the z-axis
$\bar{c}$	=	Characteristic length of the model
DCM_{be}	=	Direction cosine matrix from earth to body frame
F	=	Forces
g	=	Acceleration due to gravity
I	=	Inertia matrix
M	=	Moments
m	=	Initial mass

[1] Pathways Appointee, Atmospheric Flight and Entry Systems Branch, Student Member AIAA
[2] Research Engineer, Atmospheric Flight and Entry Systems Branch, Senior Member AIAA
[3] Research Engineer, Dynamic Systems and Controls Branch
[4] Professor, Department of Mechanical and Aerospace Engineering, Associate Fellow, AIAA

T	=	Temperature (K)
P_0	=	Ambient Air Pressure
$[p, q, r]$	=	Body rotation rates
$[p_0, q_0, r_0]$	=	Initial body rotation rates
Q	=	Measured dynamic pressure in psf
$\bar{q}$	=	Dynamic pressure in the simulation
$\hat{q}$	=	Nondimensionalized combined q and $\dot{\alpha}$
$[R_X, R_Y, R_z]$	=	Rotations in the VST reference frame
$\hat{r}$	=	Nondimensionalized combined r and $\dot{\beta}$
V	=	Measured airspeed in feet per second
V_b	=	Velocity of the model in the body frame
T	=	Temperature in degree F
T_1	=	Transformation matrix
T_{dew}	=	Dewpoint in degrees F
$[T_X, T_Y, T_z]$	=	Rotations in the VST reference frame
$[u_0, v_0, w_0]$	=	Initial velocity of the body axes
V	=	Measured airspeed in feet per second
V_b	=	Velocity of the model in the body frame
V_e	=	Velocity in Earth Reference Frame
X_e	=	Position in Earth Reference Frame
ρ	=	Air density
V_0	=	Initial airspeed of Tunnel
$[x_e, y_e, z_e]$	=	Initial position in inertial axes
$[\phi_0, \theta_0, \psi_0]$	=	Initial Euler orientation
α	=	Incidence
β	=	Sideslip
$[\phi\ \theta\ \psi]$	=	Euler rotation Angles
ω_b	=	Angular rate in body-fixed axes
$d\omega_b/dt$	=	Angular accelerations

II. Introduction

Dynamic stability analysis of atmospheric entry vehicles is essential for vehicle characterization and trajectory analysis. Currently, NASA Langley Research Center (LaRC) performs dynamic stability testing at multiple facilities on site and depending on requirements, at other locations [1]. Interest in this paper is placed on comparing the uncertainty and accuracy of some of the dynamic stability testing facilities available on center with the newly updated NASA/ODU 6-inch Magnetic Suspension and Balance System (MSBS) with its companion subsonic wind tunnel. In its current configuration, the MSBS provides a unique pseudo-free flight capability for dynamic stability testing. In this paper, emphasis will be placed on comparison of MSBS performance to several of the techniques currently available on center. These techniques are Free Flight (FF) testing as conducted in the NASA Langley Vertical Spin Tunnel (VST) as well as Free-to-Oscillate (FTO) and Forced Oscillation (FO) testing conducted in the NASA Langley Transonic Dynamics Tunnel (TDT). For this to be accomplished, simulations for each testing technique were created in MATLAB/Simulink and designed to simulate a particular facility as closely as possible.

III. Wind Tunnel Survey

To accurately design the necessary simulations for each testing environment, a thorough understanding of each facility was needed.

NASA/ODU Magnetic Suspension and Balance System

The NASA/ODU Magnetic Suspension and Balance System (MSBS) is a water-cooled electromagnetic balance installed in a low-speed subsonic wind tunnel. When the full capability of the MSBS enabled tunnel is achieved, it can generate airflows up to Mach 0.5 [2]. Levitation of a model with a magnetic core should allow for a free-to-oscillate or free flight test where the model is held in place and allowed to pivot on what is essentially a frictionless bearing [3]. Dynamic pressure within the test section is determined by measuring the difference in static pressures

across the 20:1 contraction with a calibration factor applied [2]. A camera system and dot tracking algorithm are utilized to collect angular rotation information and an Electromagnetic Positioning Sensor (EPS) is used to capture the position of the model in the test section.

The MSBS electromagnets are comprised of three separate coil systems: the Helmholtz-coil System (HCS), the Saddle-coil system (SCS), and the Side and Lift coil system (SLCS) [4][5][6]. Each coil system is responsible for controlling the electromagnetic field in a specific set of directions. The HCS is the primary axial magnetizing coil which was originally used to control the drag forces on models within the tunnel test section, also referred to as the $\overline{B_X}$ and $\overline{B_{XX}}$ directions. The SCS is responsible controlling the transverse field components, also referred to as the $\overline{B_Y}$ and $\overline{B_Z}$ directions. The SLCS is utilized to provide control over the transverse field gradients $\overline{B_{XY}}$ and $\overline{B_{ZX}}$. They are designed to coincide within one another with the SCS mounted inside the HCS with the SCLS mounted around the SCS and HCS magnet pairs. These systems are powered by a combination of a $45kW$ and 30 kW DC power supplies that feed an array of 7 power amplifiers [1]. These power amplifiers can provide up to 120A of continuous current to the coils. One of the power amplifiers is used to power the HCS while the remaining five provide dedicated services to the SCS and SLCS with three servicing the SCS and two servicing the SLCS [1]. The test section of the tunnel has a tapered hexagonal shape that is nominally 6-1/4 in across the flats. The tunnel is configured to be an open circuit

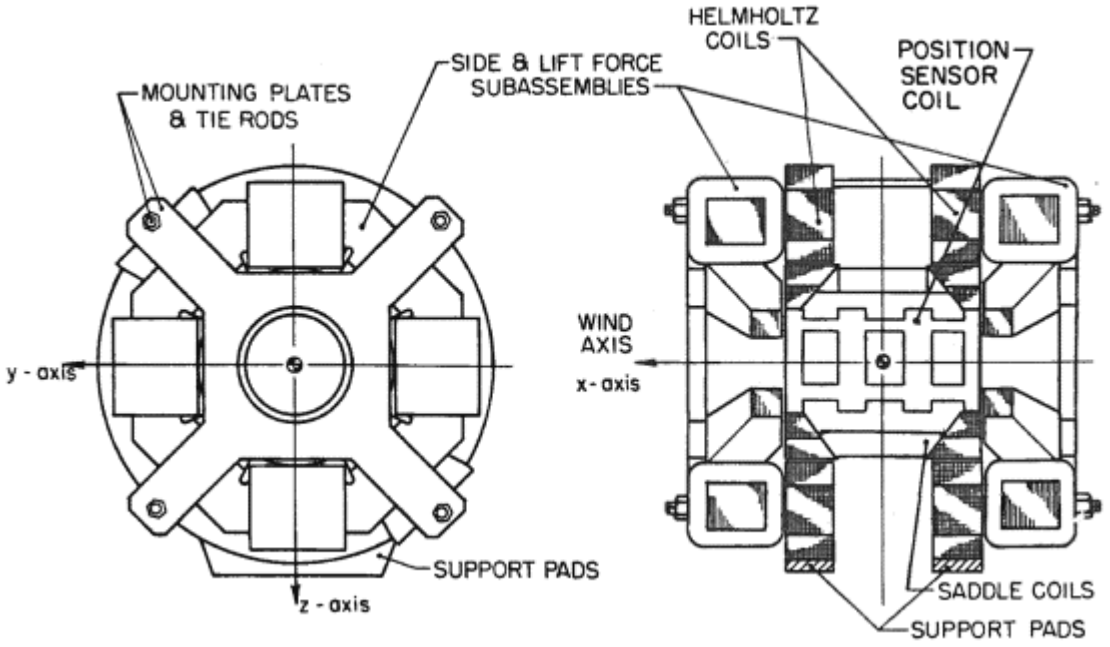

Figure 4: Magnet configuration of the Magnetic Suspension and Balance System

wind tunnel that operates at ambient pressure and temperature. The control system is driven by a Speedgoat™ target machine that is programmed through MATLAB/Simulink and controls the power supplied to the tunnel based on state information collected by the Data Acquisition System (DAQ). The DAQ system is comprised of a dynamic pressure probe to collect airflow data, a camera system to collect orientation information that is utilized in post-processing, and an Electromagnetic Position Sensor (EPS) to collect real-time position information [7][8]. Dynamic stability testing within the MSBS is achieved via controlled position magnetic levitation of the magnetic model core while allowing the model to oscillate freely in the yaw degree of freedom in the current configuration. This essentially creates a controlled 3 DOF test that allows for aerodynamic moment information to be extracted from the collected data [1]. Noise in the system can be found in the dynamic pressure readings as well as input and output errors from the power supply and power amplifiers. The EPS is also susceptible to noise as well and a vibrational analysis on the impact of the motor drive may also be required. The magnetic field symmetry within the test section has been measured and corrected for however, may still generate measurement error.

Currently data reduction involves a calibrated response to characterize the MSBS for the base power loads, currents, and controller for the desired model mass and inertia properties using a wind off data set. This data set is then utilized to create a transfer function that characterizes the baseline outputs of the MSBS. Once this is done, a second transfer function is created based on the experimentally obtained data set. This allows the built-in MATLAB System Identification toolbox to estimate the aerodynamic coefficients using the linear ordinary differential equation grey-box model with identifiable parameters.

NASA LaRC Vertical Spin Tunnel

The Vertical Spin Tunnel (VST) is a 12-sided vertical wind tunnel with a 20-foot diameter test section when measured from the flat portions of side walls of the tunnel test section. The test section has an area of approximately 300 ft^2 and is 25 feet in length. Maximum sustainable wind speeds in the VST are approximately 25 m/s [9]. The physical characteristics of the VST are shown in Figure 1. The fan motor drive is capable of sustained power outputs of 400 HP but can also generate up to 1300 HP in short bursts [8].

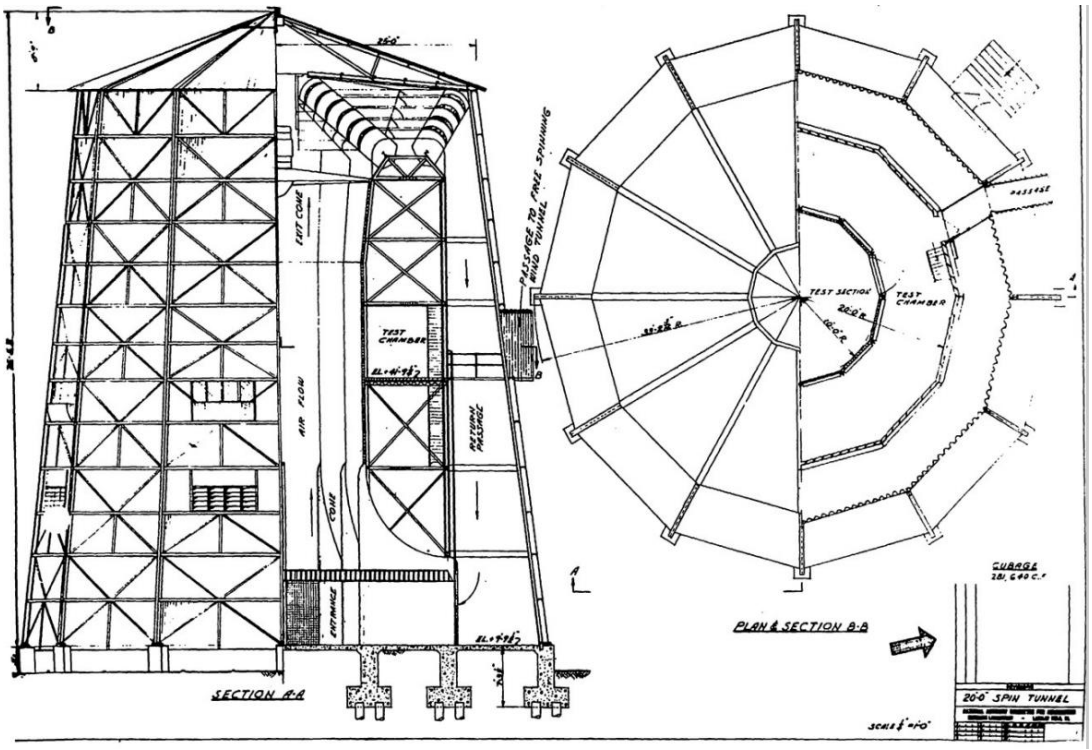

Figure 1: Overview image of the NASA Langley Vertical Spin Tunnel and its dimensions

The VST is primarily design to conduct proprietary spin-and-tumble air vehicle experiments. However, it also has the capability to aid in the assessment of dynamic stability characteristics of blunt bodiess. While the VST is outfitted to provide forced oscillation dynamic stability testing capabilities, this paper will analyze the VST's free flight dynamic stability testing mode. The data acquisition system of the VST is a non-intrusive system that consists of eight digital cameras that track the model within the test section utilizing an asymmetrical pattern of reflective targets place on the model [10]. The positions of the reflective targets relative to the nose of the model must be known so that the tracking algorithm can resolve the position and the orientation of the vehicle relative to the origin of the wind tunnel. The data obtained from conducting testing within the VST is shown in Table 1. Dynamic pressure is measured using a dynamic pressure probe located at the top of the test section which is downstream of the test vehicle.

Prior to conducted data analysis on obtained results, it is important to note that testing within the VST presents a difficulty in test run replication. This is because free flight testing is dependent on two separate human test operators. The first operator releases the model into the test section once the desired airspeed is obtained. The second manually controls the airspeed within the test section and adjusts the flow rate as needed to maintain flight within the test region for as long as possible so that data can be acquired. As a result, exact run replication is not feasible for free flight testing in the VST. The uniqueness of experimental runs can impact the statistical power of any obtained dynamic

stability parameters and recludes the possibility of employing Design of Experiments (DOE) methods to help improve understanding.

Measurement errors are also present within the collected data. Noise can be generated within the proprietary algorithm that produces the time history of the vehicle state. These errors can be compounded upon once data reduction is conducted as the vehicle translational and rotational velocities and accelerations must be determined from the body rotation and position time histories. This can greatly impact the derived aerodynamic forces and moments that are utilized to determine dynamic stability parameters. Another source of error that is rather unique to the VST when compared to the other testing facilities being researched in this work is the impact of the fan blade passing frequency on the dynamic pressure measurements that are utilized to determine the measured airspeed. Frequency analysis performed on the dynamic pressure data obtained from previous test results has shown that the dynamic pressure data includes frequencies that match the estimated fan blade passing frequencies. As a result of the dynamic pressure sensor being located at the top of the test section, the unsteady airflow surrounding the fan blade as it generates airflow can apparently impact the obtained values.

$Variable$	Definition
R_X	Body rotation about X axis in degrees
R_Y	Body rotation about Y axis in degrees
R_Z	Body rotation about Z axis in degrees
T_X	X position of model CG in tunnel frame
T_Y	Y position of model CG in tunnel frame
T_Z	Z position of model CG in tunnel frame
RPM	Rotations per minute of VST fan
V	Measured Airspeed in feet per second
Q	Measured dynamic pressure in pounds psf
T	Temperature in degrees F
T_{dew}	Dewpoint in degrees F
P_0	Atmospheric pressure in psf

Table 1: Values obtained from Vertical Spin Tunnel testing.

The appropriate data reduction technique for characterizing the aerodynamics of a flight vehicle using free flight testing in the vertical spin tunnel has been well documented by Sykes [11]. The first step is smoothing of the data. The data as provided is noisy and as a result, can generate discontinuities when evaluating derivatives that can result in faulty results. To smooth the data, a Fourier series reconstruction is performed. To accomplish this, the System Identification Programs for Aircraft (SIDPAC) MATLAB software package is utilized [12]. Fourier reconstruction generates a series of sine and cosine waves with discrete frequencies and amplitudes that when summed together can generate a nearly identical signal to the initial data set with all frequencies and noise included. As the signal is now recreated as a series of known trigonometric functions, derivatives can be obtained by analytically differentiating the corresponding trigonometric functions. However, to optimize the signal and remove the frequencies that correspond to noise, the software deploys what is known as a Wiener filter. The Wiener filter determines an appropriate cutoff frequency for a signal and when the Fourier transform is performed while omitting any sine or cosine functions for frequencies above the cutoff frequency, the raw signal becomes a continuous, smoothed, and somewhat "denoised" signal.

Once the smoothing process is completed, the signals are then optimized for data reduction. The first step that must be performed in the data reduction is the determination of the first and second derivatives of the tunnel generated position and rotation time histories. The vehicle rotational velocities and rotational accelerations can be determined by using Equations (1) and (2) respectively. The vehicle translation velocities and accelerations can be determined by using a first and second order finite differencing scheme on position time history respectively and applying Equations (3) through (7) [13]. Equation (3) shows how one can transfer the derived velocity of the origin in the body fixed coordinate system to the vehicle center of gravity by summing it with the cross product of the rotational velocities and the vector from the origin of the body frame and the center of mass. It is important to note that the velocities of the origin of the

$$[\omega] = \begin{bmatrix} p \\ q \\ r \end{bmatrix} = \begin{bmatrix} \cos R_Y \cos R_Z & \sin R_Z & 0 \\ -\cos R_Y \cos R_Z & \cos R_Z & 0 \\ \sin R_Y & 0 & 1 \end{bmatrix} \begin{bmatrix} \dot{R_X} \\ \dot{R_Y} \\ \dot{R_Z} \end{bmatrix} \quad (1)$$

$$[\dot{\omega}] = \begin{bmatrix} \dot{p} \\ \dot{q} \\ \dot{r} \end{bmatrix} = \begin{bmatrix} -\dot{R_Y}\sin R_Y \cos R_Z - \dot{R_Z}\cos R_Y \sin R_Z & \dot{R_Z}\cos R_z & 0 \\ \dot{R_Y}\sin R_Y \sin R_Z - \dot{R_Z}\cos R_Y \cos R_Z & -\dot{R_Z}\sin R_z & 0 \\ \dot{R_Y}\cos R_Y & 0 & 0 \end{bmatrix} \begin{bmatrix} \dot{R_X} \\ \dot{R_Y} \\ \dot{R_Z} \end{bmatrix} \tag{2}$$

$$+ \begin{bmatrix} \cos R_Y \cos R_Z & \sin R_z & 0 \\ -\cos R_Y \cos R_Z & \cos R_z & 0 \\ \sin R_Y & 0 & 1 \end{bmatrix} \begin{bmatrix} \ddot{R_X} \\ \ddot{R_Y} \\ \ddot{R_Z} \end{bmatrix}$$

$$U = U_0 + \omega \text{ x } r_{cm} \tag{3}$$

$$\begin{bmatrix} u \\ v \\ w \end{bmatrix} = \begin{bmatrix} u_0 \\ v_0 \\ w_0 \end{bmatrix} + \begin{bmatrix} 0 & -r & q \\ r & 0 & -p \\ -q & p & 0 \end{bmatrix} \begin{bmatrix} x_{cm} \\ y_{cm} \\ z_{cm} \end{bmatrix} \tag{4}$$

$$\begin{bmatrix} \dot{u} \\ \dot{v} \\ \dot{w} \end{bmatrix} = \begin{bmatrix} \dot{u_0} \\ \dot{v_0} \\ \dot{w_0} \end{bmatrix} + \begin{bmatrix} 0 & -\dot{r} & \dot{q} \\ \dot{r} & 0 & -\dot{p} \\ -\dot{q} & \dot{p} & 0 \end{bmatrix} \begin{bmatrix} x_{cm} \\ y_{cm} \\ z_{cm} \end{bmatrix} \tag{5}$$

$$\begin{bmatrix} u_0 \\ v_0 \\ w_0 \end{bmatrix} = [T_1]^T \begin{bmatrix} \dot{X} \\ \dot{Y} \\ \dot{Z} \end{bmatrix} \tag{6}$$

$$\begin{bmatrix} \dot{u_0} \\ \dot{v_0} \\ \dot{w_0} \end{bmatrix} = \left[\dot{T_1}\right]^T \begin{bmatrix} \dot{X} \\ \dot{Y} \\ \dot{Z} \end{bmatrix} + [T_1]^T \begin{bmatrix} \ddot{X} \\ \ddot{Y} \\ \ddot{Z} \end{bmatrix} \tag{7}$$

$$[T_1] = \begin{bmatrix} \cos R_Z \cos R_Y & -\sin R_Z \cos R_Y & \sin R_Y \\ \cos R_Z \sin R_Y \sin R_X + \sin R_Z \cos R_X & \cos R_Z \cos R_X - \sin R_Z \sin R_Y \sin R_X & -\cos R_Y \sin R_X \\ \sin R_Z \sin R_X - \cos R_Z \sin R_Y \cos R_X & \sin R_Z \sin R_Y \cos R_X + \cos R_Z \sin R_X & \cos R_Y \cos R_X \end{bmatrix} \tag{8}$$

body fixed coordinate frame are produced when multiplying the direct derivatives of the position time histories with the appropriate transformation matrix. The acceleration is determined in a similar manner and requires the derived velocities and accelerations to be multiplied with the derivative of the transformation matrix and the original transformation matrix as shown in Equation (7). The transformation matrix provided in Equation (8).

$$F = m\dot{V_b} + \omega \text{ x } mV_b = m \begin{bmatrix} \dot{u} + qw - rv \\ \dot{v} + ru - pw \\ \dot{w} + pv - qu \end{bmatrix} \tag{9}$$

$$M = I\dot{\omega} + \omega \text{ x } I\omega \tag{10}$$

Once the time histories for the rotational and translation velocities and accelerations have been obtained. It is possible to generate a time history for the total forces and moments with Equations (9) and (10). From these total forces and moments, one must remove any additional forces and moments such as the gravitational forces. Once this is completed, one is left with a time history of the aerodynamic forces and moments. From this point it is possible to apply System Identification (SID) practices such as least squares regression and the appropriate data matrix to obtain the aerodynamic coefficients that characterize the aerodynamics of the tested model, including the damping coefficients [12].

NASA LaRC Transonic Dynamics Tunnel

The NASA LaRC Transonic Dynamics Tunnel is designed to operate with blunt-body capsule geometries and conduct multiple forms of oscillatory testing. This is accomplished through the utilization of a sting and motor and an accompanying 6 degree of freedom (6DOF) force balance system that measures aerodynamic forces and moments when appropriately calibrated and installed prior to testing. Unlike both the MSBS wind tunnel and VST, the TDT is capable of testing in transonic and supersonic flows up to Mach 1.12 when heavy gas, R-134a, is utilized [14]. However, the simulations of the TDT are currently designed to operate in the subsonic flow regime as to allow for more direct comparison of results between the range of test facilities.

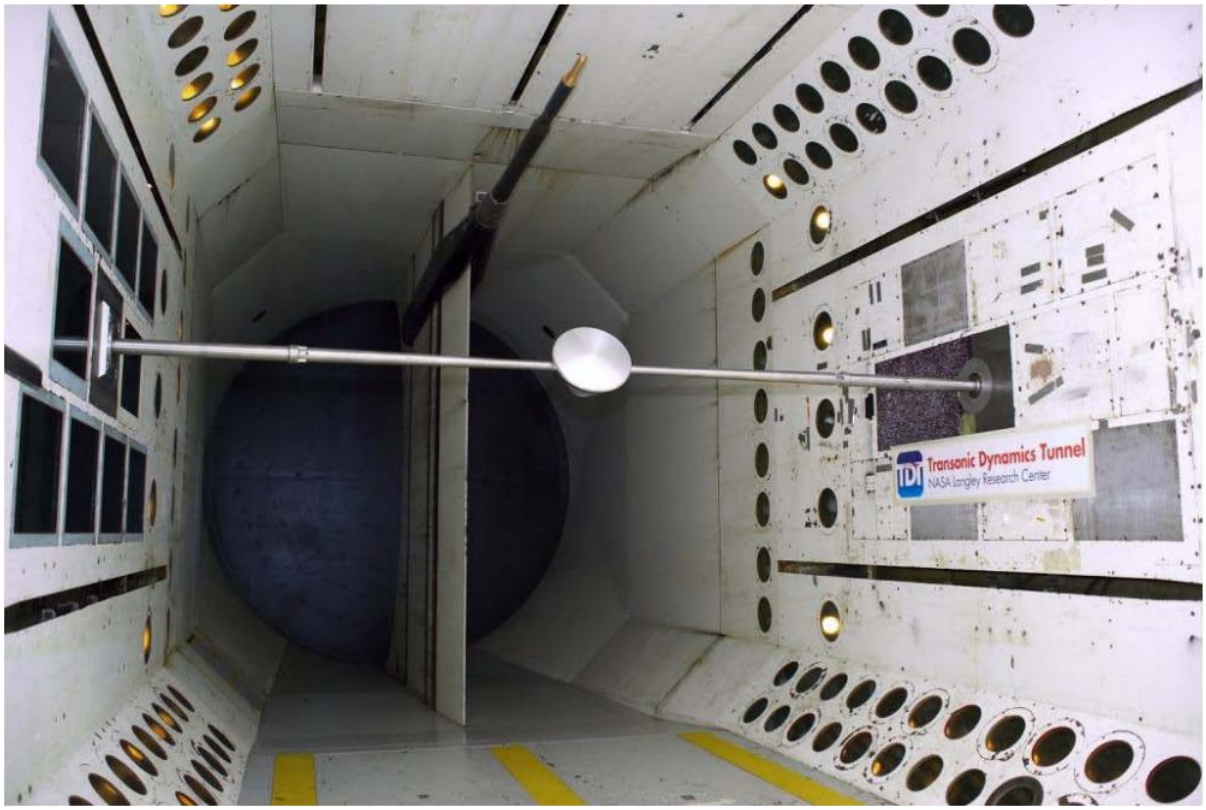

Figure 2: A scaled model mounted on the traverse sting utilized for forced and free-to-oscillate testing in the NASA Langley Transonic Dynamics Tunnel [17]

There are two primary forms of oscillatory testing that are analyzed in this work [15]. The first is the free-to-oscillate (FTO) test in which the model, balance system, and sting are placed in the tunnel at an initial angle of attack and a desired airflow. The model is then released and allowed to freely oscillate in the tunnel in the pitch degree of freedom. In doing so, the angle of attack, or alpha, time history is recorded alongside the force and moment data. This allows for data reduction to be performed.

The other two forms of oscillatory testing are remarkably similar to one another as both are forced oscillation (FO) methods. However, when forced oscillation testing is conducted, it is possible to constrain either the motion range, or it is possible to constrain the applied torque that is input into the sting to generate rotations. While both generate an alpha and force and moment time history, there are subtle differences in the noise sources that can cause slight variations in the recovered aerodynamic coefficients.

As the forces and moments are more readily available, data processing more straight-forward than when performed on data obtained in the VST or the MSBS. However, to isolate the aerodynamically generated forces and moments from the inertial forces and moments, a tare must be performed prior to testing [16]. This tare is a sweep of alphas with the wind off that can then be subtracted from the wind on measurements. Similarly, the data processing begins with the smoothing and denoising process described in the VST. Figure 3 shows a sample alpha time history obtained from the TDT FTO simulation that is then smoothed and the estimated noise vector. The accuracy of the smoothed

vector and the magnitude of the noise can be optimized with more effort in the Fourier transform frequency cutoff selection.

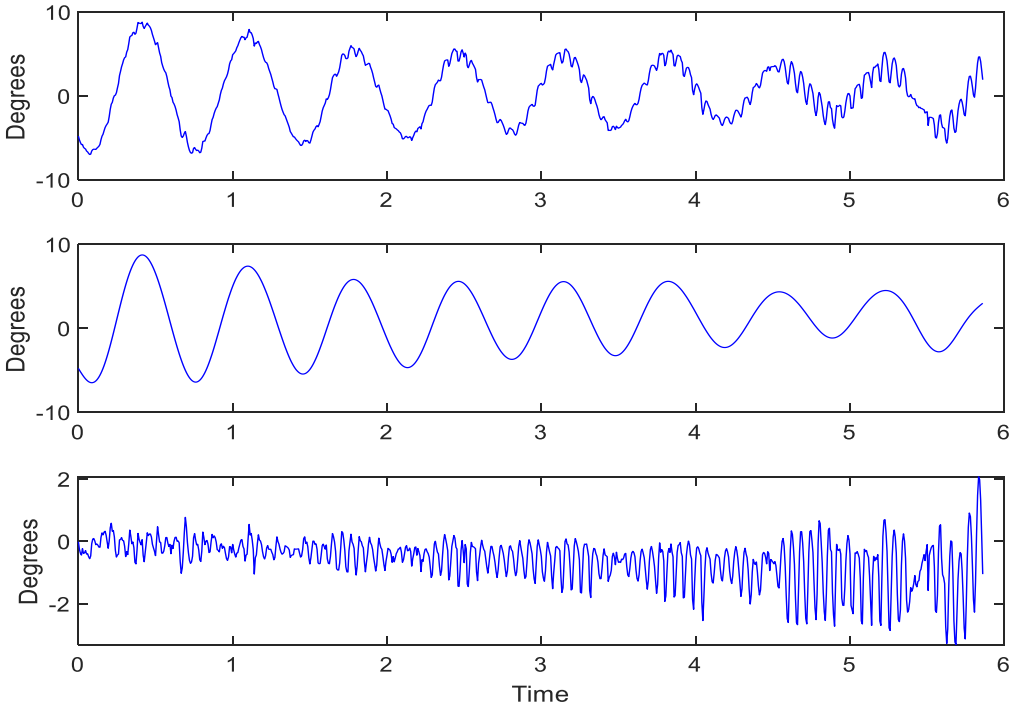

Figure 3: A Sample oscillation time history from a dynamic stability test, the recovered denoised signal through the Fourier technique, and the residual noise in the signal.

What follows the smoothing process can be one of three separate methods of obtaining the aerodynamic coefficients, or more specifically, the dynamic stability derivatives [12][17][18]. They are more commonly known as the linear dynamic derivative model, the integration method, and the specific point method. The linear dynamic derivative model requires a hypothesized aerodynamic model that contains a dynamic stability coefficient for it to be estimated. Once the hypothesized aerodynamic model is obtained, the dynamic stability coefficients and other aerodynamic coefficients that characterize the aerodynamic moment about the axis being observed can be obtained by way of SID processes like least squares regression. The integration method is accomplished by integration of the balance measurements over several complete oscillations. The mean pitching moment value of the range is determined by utilizing Equation (11). The in-phase $\overline{C_{m_\alpha}}$ and out-of-phase $\overline{C_{m_q}}$ can be obtained through mathematical manipulation of Equation (11) to arrive at Equations (12) and (13) respectively. It is important to note, that the integration method is dependent upon the integration of the moments of complete cycles, utilization of incomplete cycles can introduce errors as the extracted values will be biased towards one of the sides of the alpha sweep rather than provided values at the mean alpha. The third method of data reduction is referred to as the specific point method. The specific point method relies on taking the measured moments at the maximum and minimum angular rates as well as the point of zero angular acceleration. Once these values are known, the moments at the minimum angular rate are subtracted from the moments at the maximum angular rate, following the procedure presented in Equations (14) through (16).

$$C_{m_0}(\alpha_0) = \frac{1}{\bar{q}S\bar{c}} \int_{t_0}^{t_0+T} [M_b(t) - M_k(t)]dt \tag{11}$$

$$\overline{C_{m_\alpha}} = \frac{2}{\bar{q}S\bar{c}AT} \int_{t_0}^{t_0+T} [M_b(t) - M_k(t)] \sin(\omega t)\, dt \tag{12}$$

$$\overline{C_{m_q}} = \frac{4V}{\bar{q}S\bar{c}^2\omega AT}\int_{t_0}^{t_0+T}[M_b(t) - M_k(t)]\cos(\omega t)\,dt \tag{13}$$

$$C_{m_0}(\alpha_0) = \frac{1}{2}\frac{(M_a(q_{max}) - M_a(q_{min}))}{\bar{q}S\bar{c}} = \frac{1}{2}[C_m(q_{max}) + C_m(q_{min})] \tag{14}$$

$$\overline{C_{m_q}}(\alpha_0) = \frac{V}{\bar{c}A\omega}\left[\frac{M_a(q_{max}) - M_a(q_{min})}{\bar{q}S\bar{c}}\right] = \frac{V}{\bar{c}A\omega}[C_m(q_{max}) + C_m(q_{min})] \tag{15}$$

$$\overline{C_{m_\alpha}}(\alpha_0) = \frac{-1}{2A}\left[\frac{M_a(\dot{q}_{max}) - M_a(\dot{q}_{min})}{\bar{q}S\bar{c}}\right] = \frac{-1}{2A}[C_m(\dot{q}_{max}) - C_m(\dot{q}_{min})] \tag{16}$$

More commonly than not, this work will refer to the linear dynamic derivative method that utilizes SID. This is to minimize numerical errors and discrepancies in values that can be attributed to the method of data reduction.

Other facilities

From time-to-time, LaRC researchers will use the Aeroballistic Research Facility at Eglin Air Force Base or the Transonic Experimental Facility in Maryland [19]. These tests are performed by way of ballistic range techniques. Scaled models are fitted with dynamic pressure sensors on the aft bodies. Once manufactured, they will be placed into an appropriate powder charge gun and fired supersonically. Data stations along the range take shadowgraph images that help determine the vehicle velocity and trajectory. The recovered trajectory, velocity, and pressure information is utilized to determine aerodynamic characteristics. Full analysis of these facilities is beyond the scope of the current paper.

IV. Simulation Design

The simulations were built up utilizing the built-in Simulink Aerospace Blockset and custom created subsystems [20]. Each simulation is comprised of multiple subsystem blocks that are designed to act according to the needs of each individual test method. The subsystem blocks are referred to as the primary blocks and are created to simulate the tunnel control, the nonlinear 6DOF simulation, a data acquisition block, and when required, a camera system block. Each simulation is initiated by a MATLAB script that creates initial conditions, model parameters, constants, and simulation settings. Once these values are set, the script runs the simulation, accordingly, stores the output data, and performs the appropriate data reduction procedures to acquire the aerodynamic coefficients. It is important to note that the simulations are initiated with a set of aerodynamic coefficients that are referred to as the true values. The simulations are then run with additional noise to simulate the noise in the physical testing environment. This noise will then impact the recovered coefficients. The deviation from the true values utilized to initiate the simulations will be utilized to determine the overall accuracy of each test method and determine the sensitivity of the experimentally obtained dynamic stability coefficients to each individual source of noise.

CG	Center of Gravity
CP	Center of Pressure
T	Temperature (K)
P_0	Ambient Air Pressure
ρ	Air density
V_0	Airspeed of Tunnel
$[x_e, y_e, z_e]$	Initial position in inertial axes
$[u_0, v_0, w_0]$	Initial velocity of the body axes
$[\phi_0, \theta_0, \psi_0]$	Initial Euler orientation
$[p_0, q_0, r_0]$	Initial body rotation rates
m	Initial mass
I	Inertia matrix

Table 2: Values that are used to initiate the aerodynamic of the 6 degree of freedom simulation.

Simulink Aerospace Blockset

The Simulink Aerospace Blockset plays a large part in the aerodynamics and trajectory portions of all the simulations. At the root of it all is the nonlinear 6DOF fixed mass body quaternion block [20]. The nonlinear 6DOF fixed mass body quaternion block takes the required initial conditions shown in Table 2 and generates the values presented in Table 3 for the next timestep. It does this by solving the aircraft 6DOF equations of motion such as Equations (9) and (10) to determine the rotational and

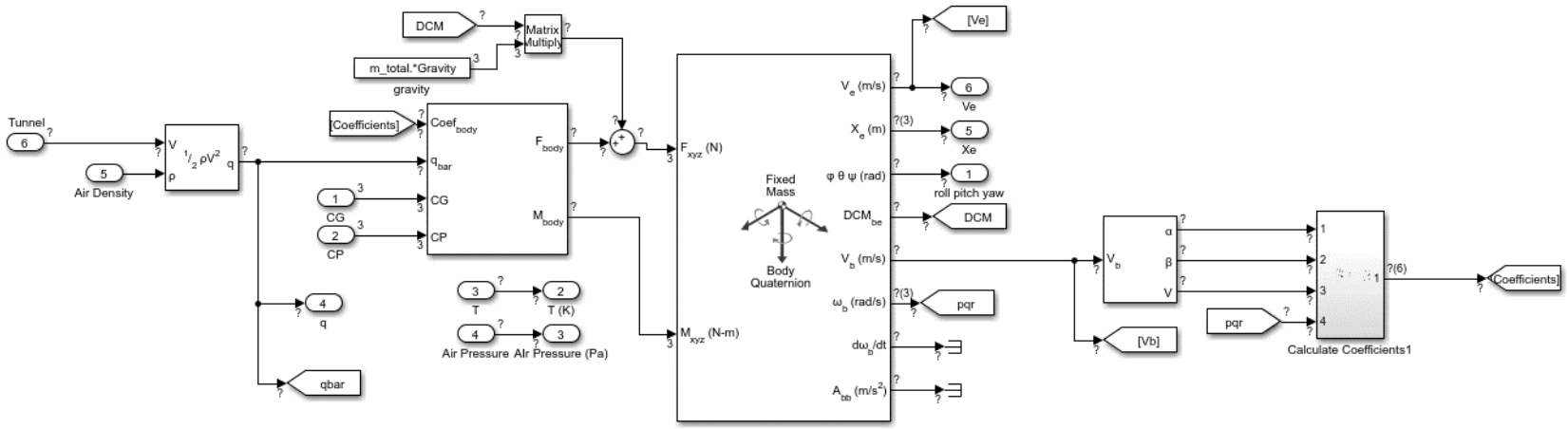

Figure 4: Overview of the 6 degree of freedom simulation

V_e	Velocity in Earth Reference Frame
X_e	Position in Earth Reference Frame
$[\phi\ \theta\ \psi]$	Euler rotation Angles
DCM_{be}	Coordinate transformation
V_b	Velocity in the body fixed-frame
ω_b	Angular rate in body-fixed axes
$d\omega_b/dt$	Angular accelerations
A_{bb}	Accelerations in body-fixed axes

Table 3: Values that generated by the fixed mass body quaternion block of the built in Simulink Aerospace Blockset.

translational velocities and acceleration from the incoming total forces and moments while assuming constant mass and a known inertia matrix. Once this is done, the body orientation and state are then integrated via quaternions to arrive at the next estimated vehicle state.

With the state now known, the velocity in the body frame is then passed to the incidence, sideslip, and airspeed block. These values are required to determine the aerodynamic coefficients. The incidence, sideslip, and airspeed are then passed into the custom created coefficients block along with the angular rate in the body-fixed axes that is calculated by the nonlinear 6DOF fixed mass body quaternion block. In the coefficients block, the aerodynamic coefficients are updated according to the true values that were utilized to initiate the simulation. Once the coefficients for the current state of the vehicle are determined, the coefficients are utilized in conjunction with the dynamic pressure, the CG, and the CP to determine the aerodynamic forces and moments. Gravitational forces are then determined by multiplying the direction cosine matrix with the gravitational force vector. With the total forces and moments of the next time step now determined, the initial 6DOF block can begin the process of updating the state of the vehicle for the next timestep. The overall process described is illustrated in Figure 4.

In most instances, the tunnel speed block is simply a straightforward setting that is generated by the MATLAB script. Turbulence is then added according to available facility literature that characterizes the condition of the flow within each test section. This flow is then utilized to determine the dynamic pressure history in the tunnel. The data acquisition block is most typically a simply pass through that accept output values of the simulation that replicate the values obtained by the facility data acquisition systems. The dynamic pressure time history has noise added according to manufacturer's specifications of the data acquisition equipment utilized in each system. For the simulations that utilize a 6DOF strain gage balance, the values obtained from the simulation are corrupted with white noise that meets standard calibration practices as determined by the National Institute of Standards and Technology. The exception to this is the camera algorithm block that is unique to the VST free flight simulation.

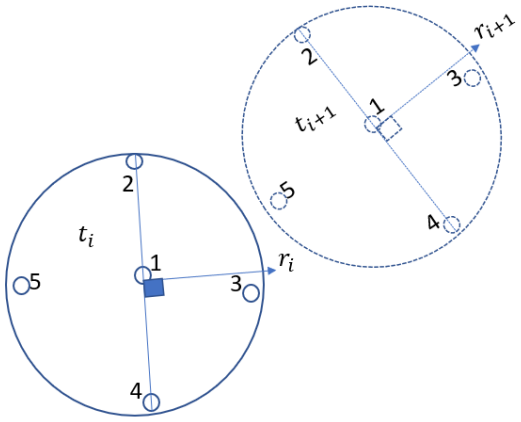

Figure 5: Image depicting the angle recovery method.

To replicate the data outputs of the VST testing environment a user defined trajectory recovery algorithm had to be created. The tunnel system uses the proprietary VICON camera system algorithm. A standard asymmetric dot pattern was used. These positions of the dots relative to the nose of the model were entered into the MATLAB script. The positions of the dots were then updated at each timestep based on the vehicle body state. From there, the positions of these dots were transferred to the relative position according to each camera in the camera system. A time history of each dot was then created relative to each individual camera. This created 7 separate time histories for the dots positioned on the nose of the model and a single time history for the dot position on the back shell of the model. These time histories are then corrupted with an appropriate noise level. The estimated position of all the dots is then based on the average position of all the corrupted position time histories. This new estimated dot position is then utilized to determine the vehicle velocity and acceleration. The body angles are then determined by calculating the angle between the known dot positions relative to the nose and the newly estimated positions. This is done by utilizing the dot patterns to create planes that bisect the body $x-axis$ and calculating a vector normal to this plane. The angle between this initial zero roll, pitch, yaw vector and the current state can recover an estimated angle at each time step. This recovered time history is then utilized as the output angle time histories for data reduction purposes.

The simulation for the MSBS was built to utilize many of the standard Aerospace Blockset blocks. However, the MSBS simulation also contains custom blocks that represent the control system and EPS position measurement subsystems. The magnetic forces and moments utilized to sustain levitation and maintain the model within the desired test volume are determined by means of interpolation from physically measured data obtained by utilizing a gaussmeter to measure the magnetic fields and gradients at various stations within the tunnel test section. During simulation, the gaussmeter data is utilized by means of interpolation between data sets based on the current, voltage, and position of the model within the test section. These magnetic forces and combined with the aerodynamic and gravitational forces and moments to obtain the total forces and moments that are utilized to predict the state of the vehicle at the next time step. The MSBS simulation system generates reasonably realistic trajectory and position

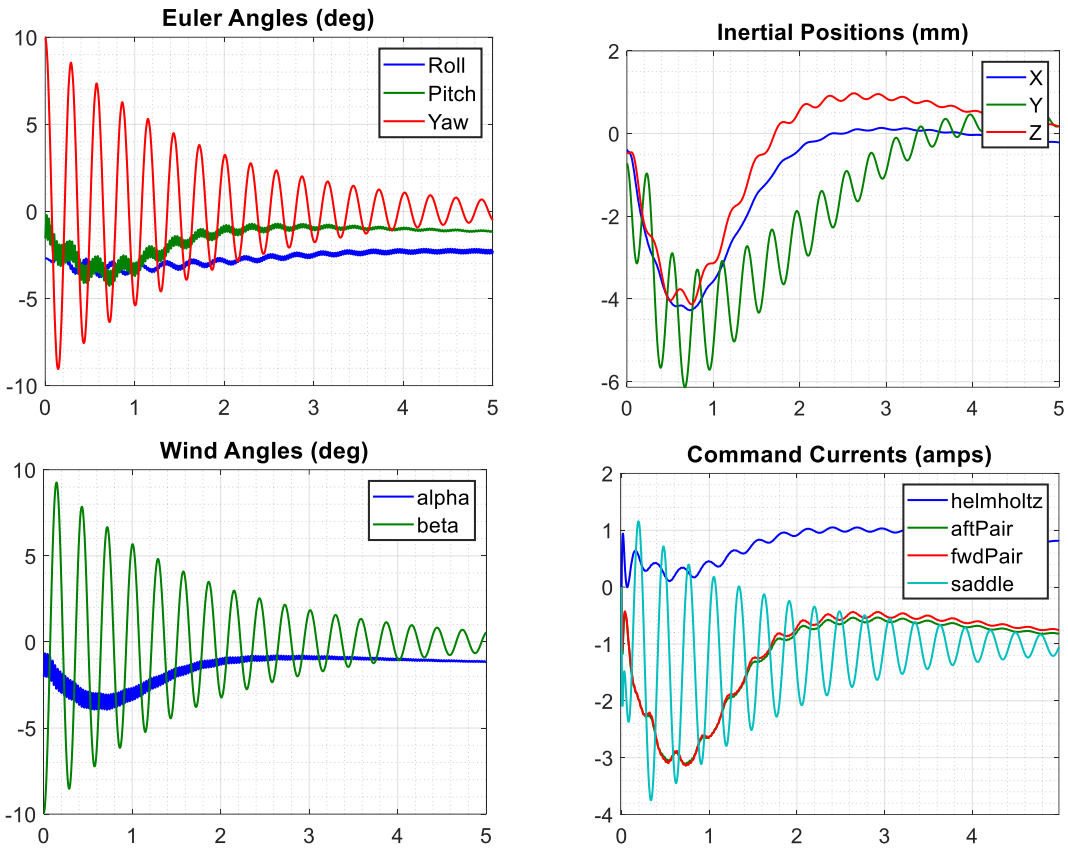

Figure 7: Sample run of data from MSBS Simulation.

tracking data. An example of data that can be obtain via simulation is shown in Figure 7. Data reduction can then be applied to the obtained simulated data to arrive at dynamic stability parameters.

V. Data Analysis

Simulated and experimentally obtained data sets were subjected to global smoothing operations and then subjected to data reduction and system identification techniques to extract dynamic stability coefficients from the results. Since the simulations are created using a predetermined set of aerodynamic parameters, any deviation from them is a direct result of the noise introduced into the results to corrupt the data. This allows for a direct interpretation of the impact for a particular source of noise on the dynamic stability results extracted as well as the uncertainties associated with each individual source of noise.

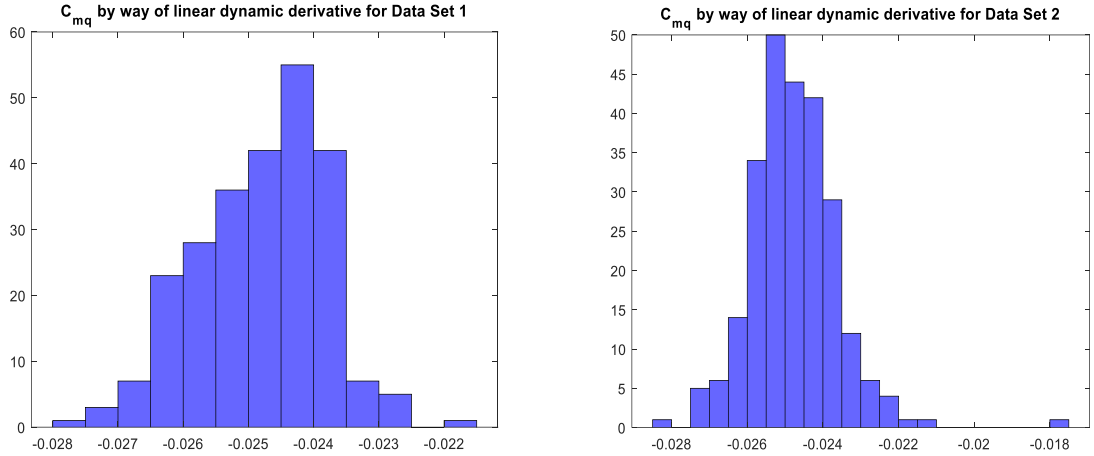

Figure 7: Histogram of C_{mq} values obtained in data sets 1 and 2.

To demonstrate the overall analysis of results a series of simulated data runs in the TDT forced oscillation constrained alpha technique will be reviewed. Two data sets were generated, one in which the mean angle of attack, sweep amplitude, and wave frequency for the simulation were kept constant and only data corruption using white noise was performed. In the second data set these values were allowed to vary in a normally distributed randomly generated manner. Each data set contains 250 simulated runs. In both data sets the determined C_{m_q} values through the linear dynamic derivative method possessed a mean value of -0.0248 based on a true initial value of -0.025. While data set 2 demonstrated similar results, the initial conditions varied significantly from the baseline values of the mean pitch angle of 4 degrees and the sweep magnitude of 10 degrees in the constant data set as shown in Figure 8. The TDT free-to-oscillate simulation generated mean C_{m_q} values of -0.0023 against a true value of -0.025 indicating that

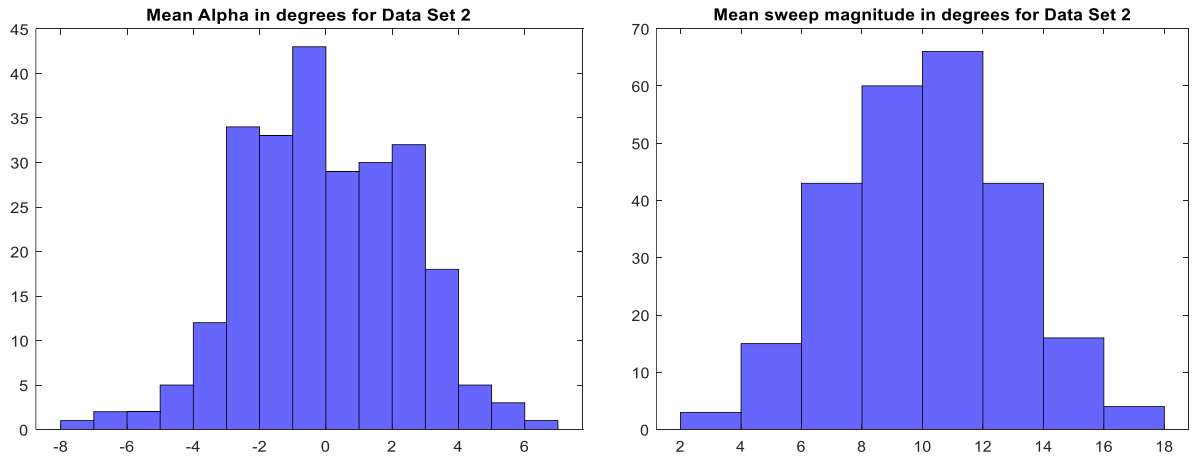

Figure 8: Histogram of mean alpha angles and sweep magnitudes for Data Set 2.

there is some differences in results between the test techniques even when they are conducted within the same facility.

The VST simulation produced more scattered values for a set of randomized initial conditions for roll, pitch, and yaw, the data for 250 runs generated a mean C_{m_q} value of approximately -0.0001 with a true value of -0.125. The C_{m_α} values fared far better producing a mean value of -0.0039 when compared to a true value of -0.003 that was extracted from the data provided by Mitcheltree et. al. [21][22][23][24]. For comparison, Figure 9 shows the data collected from a physical test of an 8-inch diameter Stardust model conducted in the VST. When reduced, the extracted value for C_{m_q} was -0.0048 and C_{n_r} was -0.0054.

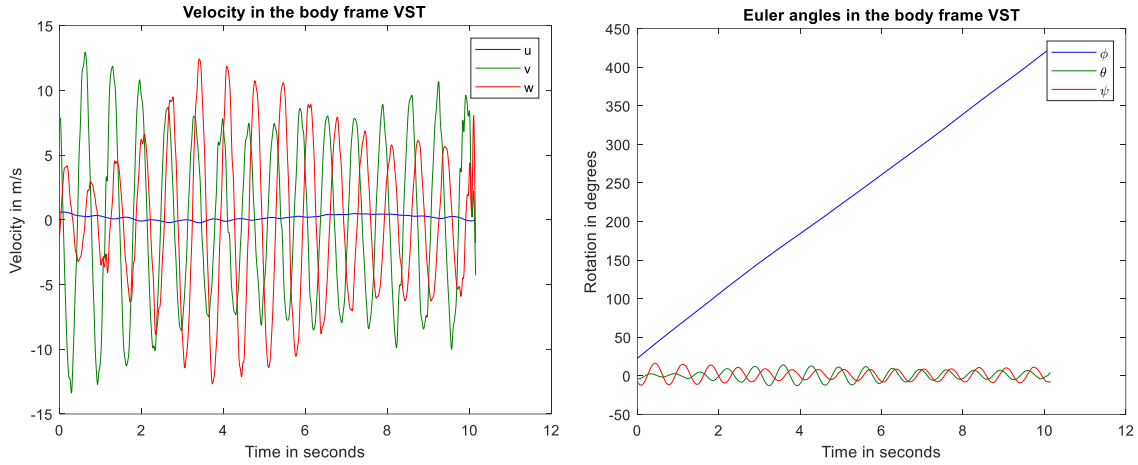

Figure 9: Histogram of mean alpha angles and sweep magnitudes for Data Set 2.

Currently, the MSBS parameter identification methods for the simulated data are a work in progress. A "compass needling" mode arises due to the lack of the close-loop control on pitch and roll in the current configuration. This mode is observed in the simulated data and is also present in the real tunnel data when testing is conducted. This compass needle mode causes systemic errors when attempting to analytically solve for body rotational velocities and accelerations. These errors significantly impact the analytically obtain total forces and moments and thereby produce errors in the results. These impacts can be reduced by determining the bias angle at which the simulation wants to maintain the roll and pitch angles. By setting the roll and pitch angles to be close to these bias values, the needling mode in the simulation can be somewhat mitigated although it is still present. System identification is possible using the two-step method of parameter identification created by Cox to some varying degrees of success and the SIDPAC least squares regression method provides reasonable values for the C_{m_α} when the compass needle mode is removed from the data set entirely. However, the least squares regression method continues to have difficulties identifying C_{m_q} values. This will continue to be an area of work moving forward

VI. Summary

Simulated test environments were created to emulate several dynamic stability test techniques available at prominent test facilities at NASA LaRC. Currently, the simulations can generate reasonably realistic simulated test results that can be analyzed in bulk to identify dynamic stability parameters. The accuracy of the forced oscillation test modes has provided results that are more accurate than the free flight testing or the free-to-oscillate testing. The largest source of errors introduced in the VST free flight simulation is in the rotation time histories generated by the custom created camera tracking algorithm. A test in being developed to aid in the overall understanding of the noise sources and their magnitude within the VST. Once completed, the free flight simulation will be updated to reflect the findings and a final analysis on the extracted dynamic stability parameters can be performed.

Further work must be done to be able to accomplish the overall goal of comparing the results obtained by the MSBS with the other testing facilities and techniques available on center at NASA LaRC. The total overall impact of individual sources of noise will be further analyzed to identify which noise source impacts the uncertainty level of the

results the greatest. This will make sure that experiments can be designed to account and mitigate the significant sources of noise thereby increasing the overall success and accuracy of the results.

References

1. Owens, D. B., Brandon, J. M., Croom, M. A., Fremaux, C. M., Heim, E. H., and Vicroy, D. D., "Overview of Dynamic Test Techniques for Flight Dynamics Research at NASA LaRC," AIAA Paper 2006-3146, 2006.
2. M. Schoenenberger, et. al., "Preliminary Aerodynamic Measurements from a Magnetic Suspension and Balance System in a Low-Speed Wind Tunnel," AIAA Applied Aerodynamics Conference, June 2018. AIAA 2018-3323.
3. C.P. Britcher, "Feasibility of Dynamic Stability Measurements of Planetary Entry Capsules Using MSBS", 12th International Conference on Flow Dynamics, ICFD2015, October 2015
4. M. Judd, "The Magnetic Suspension and Balance System as a Wind Tunnel Dynamic Balance", 3rd International Congress on Instrumentation in Aerospace Simulation Facilities, ICIASF'69, May 1969, pp:198-206
5. T. Stephens, et. al., "Recent Developments in a Wind Tunnel Magnetic Balance", 10th AIAA Aerospace Sciences Meeting, January 1972. 15. S. Abdel-Kawi, et. al. "Aerodynamic Data Acquisition with the University of Southampton Magnetic Balance," 2nd International Symposium on Electro-Magnetic Suspension, July 1971
6. C. Haldeman, et. al. "Improvements in the Magnetic Suspension and Balance System Required for Magnus Testing", 5th International Congress on Instrumentation in Aerospace Simulation Facilities- ICIASF'73, September 1973
7. T. Stephens, "An Electromagnetic Remote Model Position Sensing System for Wind Tunnels with Particular Application to Magnetic Suspension Systems", 2nd International Symposium on Electro-Magnetic Suspension, July 1971
8. T.S. Daniels, J.S. Tripp, "Improvements to an Electromagnetic Position Sensor for a Magnetic Suspension Wind Tunnel", 1988. ISA 88-0708
9. *20-foot vertical spin tunnel - NASA*. (n.d.). Retrieved November 10, 2022, from https://www.nasa.gov/sites/default/files/atoms/files/20-foot-vertical-spin-tunnel-fact-sheet.pdf
10. Glaab, Louis J. et. al., "Vertical Spin Tunnel Testing and Stability Analysis of Multi-Mission Earth Entry Vehicles," International Planetary Probe Workshop, June 2014
11. Sykes, Robert A., "Aerodynamic Parameter Identification of a Venus Lander," (2013). Graduate Theses, Dissertations, and Problem Reports. West Virginia University 612.
12. Klein, V. and Morelli, E.A. Aircraft System Identification: Theory and Practice, AIAA Education Series, AIAA, Reston, VA, 2006.
13. Osborne, M. R., "An error analysis of finite-difference methods for the numerical solution of ordinary differential equations," *The Computer Journal*, vol. 7, 1964, pp. 232–237.
14. C. Wieseman and R. Sleeper, "Measurements of Flow Turbulence in the NASA Langley Transonic Dynamics Tunnel," NASA/TM-2005-213529
15. Prislin, R. H., "Free-Flight and Free-Oscillation Techniques for Wind Tunnel Dynamic Stability Testing," National Aeronautics and Space Administration, March 1966, Technical Report No. 32-878
16. Bryant, Charles S., Hoadley, Sherwood T., "Open Architecture Dynamic Data System at Langley's Transonic Dynamics Tunnel," 36th AIAA Aerospace Sciences Meeting and Exhibit, January 1998, AIAA-98-0343
17. Owens, D. Bruce, Aubuchon, Vanessa V., "Overview of Orion Crew Module and Launch Abort Vehicle Dynamic Stability," 29th AIAA Applied Aerodynamics Conference, AIAA 2011-3504
18. N. Alemdaroglu et. al., "Determination of Dynamic Stability Derivatives Using Forced Oscillation Technique," 40th AIAA Aerospace Sciences Meeting and Exhibit, January 2002. AIAA 2002-0528
19. M. Schoenenberger, et. al., "Surface Pressure Ballistic Range Test of Mars 2020," AIAA Applied Aerodynamics Conference. June 2017. AIAA 2017-4079
20. Leong, H., "Development of a 6DOF Nonlinear Simulation Model Enhanced with Fine Tuning Procedures," Engineering Dissertations and Theses, University of Kansas, 2008

21. R Mitchletree, et. al., “Aerodynamics of Stardust Sample Return Capsule,” 15th AIAA Applied Aerodynamics Conference, July 1997. AIAA 1997-2304
22. Mitcheltree, R. A., Fremaux, C. M., “Subsonic Dynamics of Stardust Sample Return Capsule,” NASA TM 110329, March 1997
23. Wilmoth, R. G., Mitcheltree, R. A, Moss, J. N., “Low-Density Aerodynamics of Stardust Sample Return Capsule,” AIAA Paper 97-2510, June 1997
24. Mitcheltree, R. A., Fremaux, C. M., Yates, Leslie A., “Subsonic Static and Dynamic Aerodynamics of Blunt Entry Vehicles,” 37th Aerospace sciences Meeting and Exhibit January 1999, AIAA 99-1020
25. Owens, D. B., Brandon, J. M., Croom, M. A., Fremaux, C. M., Heim, E. H., and Vicroy, D. D., “Overview of Dynamic Test Techniques for Flight Dynamics Research at NASA LaRC,” AIAA Paper 2006-3146, 2006.
26. Cole, Stanley R., Garcia, Jerry L., “Past, Present and Future Capabilities of the Transonic Dynamics Tunnel from an Aeroelasticity Perspective,” AIAA Dynamics Specialists Conference, April 2000, AIAA 2000-1767
27. Williams, Brianne Y. "The Effect of Systematic Error in Forced Oscillation Wind Tunnel Test Apparatuses on Determining Nonlinear Unsteady Aerodynamic Stability Derivatives" (2010). Doctor of Philosophy (PhD), Dissertation, Mechanical & Aerospace Engineering, Old Dominion University, DOI: 10.25777/9v50-f824
28. M. Schoenenberger, L. Yates, W. Hathaway, "Dynamic Stability Testing of the Mars Science Laboratory Entry Capsule", 41st AIAA Thermophysics Conference, June 2009. AIAA 2009-3917
29. B.R. Hollis, et.al., "Entry, Descent and Landing Aerothermodynamics: NASA Langley Experimental Capabilities and Contributions", 52nd AIAA Aerospace Sciences Meeting, January 2014. AIAA 2014-1154
30. R. Oshima, H. Sawada, S. Obayashi, "A Development of Dynamic Wind Tunnel Test Techniques by Using a Magnetic Suspension and Balance System", 54th AIAA Aerospace Sciences Meeting, January 2016. AIAA 2016-1541
31. T. Stephens, "Design, Construction and Evaluation of a Magnetic Suspension and Balance Systems for Wind Tunnels", NASA CR-66903, November 1969.
32. T. Schott, T. Jordan, T. Daniels, “Present Status of the MIT/NASA Langley 6-inch MSBS”, International Symposium on Magnetic Suspension Technology, NASA CP-3152, August 1991
33. P. Tcheng, T. Schott, “A Five Component Electro-Optical Positioning System, 12thInternational Conference on Instrumentation in Aerospace Simulation Facilities, ICIASF’87, June 1987
34. Johnson, D.: "Modeling of a Wind Tunnel Magnetic Suspension and Balance System". AIAA Region I student conference, April 2017